propulsion methods are shown by plotting Eqs. (9–12) in Fig. 3.‡

To illustrate combined effects on the cost of a specific far-orbit space operation, Fig. 4 shows annual cost vs t or l using total replacement, manned maintenance, manned maintenance plus refueling, and manned maintenance plus refueling plus improved propulsion.

Observations

Earth-based manned maintenance (EBM) is economically preferable to total replacement for payloads weighing more than 500 to 3000 lb (depending on τ, n_m, etc.), essentially independent of t. Station-based manned maintenance (SBM) is preferable to EBM for $t < 0.2$ to 0.4 yr (depending on n_s, l, etc.), essentially independent of payload weight, and SBM may also be preferable to total replacement (TR) for $w_p < 500$ to 3000 lb and $t < 0.2$ to 0.4 yr. These results refer to typical near-orbit conditions, but are not much different for far-orbit cases. If payload useful life is increased without manned maintenance by improved electronic technology, the breakeven condition between TR and EBM will not change appreciably, but the preferability of EBM vs SBM will then depend on whether t or l could be extended most.

If crew duty cycle (l) can be extended to 3 to 6 months, and multiple payload servicing is done, SBM appears attractive economically (Fig. 2a), and has several inherent advantages over both TR and EBM. First, the continuous presence of man can reduce the requirements for equipment that is redundant or could be replaced by man. Second the system cost for SBM is far less sensitive to uncertainties in w_p and C_p and is essentially independent of t, whereas both TR and EBM are very sensitive to these parameters. Third, more payloads can be serviced readily by a single station equipped with maneuvering tenders, than by a single earth-based flight; in certain applications (e.g., missile launching platforms) hundreds of payloads may be serviced from each station.

For a large-payload-boost-cost reduction of 50%, refueling in near orbit can reduce the near-orbit/far-orbit/earth round trip (Δv = 18,000 fps) cost by about \$800/lb for O_2-H_2 chemical propulsion (Fig. 3a); for a 10,000+ lb. payload such as the Apollo command module, this is equivalent to a savings of nearly 10 million dollars per deep space or lunar flight. Greater savings can be obtained if nuclear propulsion is used, or if refueling is done in both near and far orbit. All such reductions in transportation cost increase the economic attractiveness of manned maintenance (Fig. 2b).

The maneuvering truck appears economically preferable only if it utilizes gas-core nuclear propulsion and for large-payload boost-cost reductions up to about 75% when compared to near-orbit refueling using O_2-H_2 chemical propulsion, and up to about 50% when compared to near-orbit refueling using gas core nuclear propulsion (Fig. 3b). Since it operates only in space, the truck might be able to utilize higher performance space propulsion such as nuclear explosion (or electric, if the increased maneuver times resulting from low thrust-to-weight ratios could be tolerated) to improve its economy. This mode, of course, would be required by definition if some need developed for the mission vehicle to return to near orbit after each trip.

For a typical far-orbit or deep space system utilizing 2500-lb payloads, if t = 0.5 yr and l = 0.5 yr, the combined use of manned maintenance, refueling and improved propulsion is shown (Fig. 4) to produce a 71% (or 20 million dollars) reduction in annual cost per payload, with each contributing about equally to the savings. Further savings could be achieved, especially in deep space operations, if lunar propellants become available, as described in Ref. 1.

‡ In all cases except the maneuvering tanker which is single-stage by definition, two-stage K values have been used where $\Delta v > 15{,}000$ for I = 450 sec and I = 850 sec cases. [For a total Δv, it can be shown that $K_{(2\text{-stage})} = K_{\Delta v/2}(K_{\Delta v/2} + 2)$.]

Reference

[1] Salkeld, R. J., "Economic Implications of Extracting Propellants from the Moon," *Journal of Spacecraft and Rockets*, Vol. 3, No. 2, Feb. 1966, pp. 254–261.

Analysis of Two-Phase Impingement from a Cryogen Vented in Orbit

E. A. Evans* and A. B. Walburn†
Convair Division of General Dynamics, San Diego, Calif.

Nomenclature

A = area
D = drag force
d_s = particle diameter
h_{fg} = latent heat of vaporization
j_{m_0} = interphase mass transport flux
k = slip ratio
M = local Mach number
$\dot{M}$ = total mass flow rate
$\dot{m}$ = mass flux
P,P_t = pressure and total pressure, respectively
$\dot{q}$ = heat flux
r,θ = radial and angular coordinates (Fig. 1)
R = gas constant
T = temperature
v = velocity; $v_g^* = (\gamma RT_*)^{1/2}$
V = volume
x = quality
α = void fraction
δ_m = percentage of second phase reduction
γ = ratio of specific heats
ϕ = angle between inward normal to impingement surface and radial vector
ρ = density
λ = interphase mass transport relaxation constant
$\theta_{\max}$ = maximum flow angle
τ = tangential surface traction

Subscripts

A,N = actual and Newtonian, respectively
$0,f$ = initial and final conditions, respectively
g,s = gas phase and second phase, respectively
n = normal
p = particle
r,θ = properties at r and θ, respectively
$*$ = choked flow property at orifice

Introduction

THIS Note addresses the problem of impingement forces on surfaces in the vicinity of a cryogen that is being vented. This problem necessitates an investigation of the local multiphase momentum flux. Using the assumption of steady flow, the problem is reduced to considering a spatially

Presented as Paper 69-571 at the AIAA 5th Propulsion Joint Specialist Conference, U.S. Air Force Academy, Colo., June 9–13, 1969; submitted May 23, 1969; revision received July 22, 1969. This study was performed under NASA-Marshall Space Flight Center Contract NAS 8-20165. The study was administered under the technical direction of the Propulsion and Vehicle Engineering Laboratory; W. Jensen acted as project manager.

* Senior Thermodynamics Engineer.
† Design Specialist.

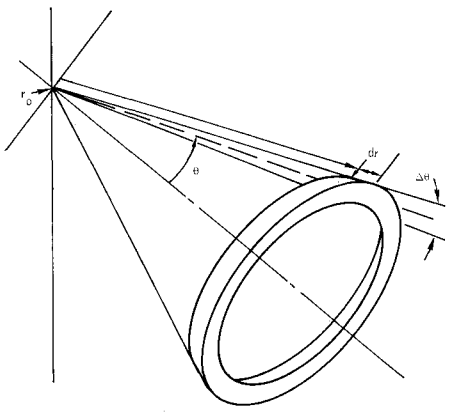

Fig. 1 Conical flowfield differential volume.

dependent, two-phase mixture with interphase mass transport and drag forces. Choked-flow conditions are assumed to exist at the orifice (vent). Using Newtonian impact theory, modified by momentum exchange considerations at the impingement surface, the impingement force is obtained from the momentum flux.

Venting of a gas into a vacuum has been studied.[1] The method of characteristics is used to map the vent gas flowfield, and Newtonian impact theory provides the corresponding force field,

$$\Delta F_N = (\gamma M^2 \cos^2\phi + 1)\{1 + [(\gamma - 1)/2]M^2\}^{\gamma/(1-\gamma)} \times P_t \Delta A \quad (1)$$

Using a correction factor of 1.15, Eq. (1) correlated very well with vacuum-chamber test data and Centaur and Saturn S-IV staged-flight orbital test data; this coefficient absorbs the inelastic surface effects.

When cryogenic liquid or liquid-gas mixture is vented into a vacuum, the liquid phase breaks up into small drops that evaporate until the droplet surface temperature reaches the triple point; freezing commences and a three-phase mixture is present; and gas generation continues through solid sublimation. During phase changes, the droplets are being accelerated by drag forces created by the expanding gas phase.

Flowfield Model and Equations

A previous investigation[1] indicated that for a gas expanding in a vacuum, the flowfield is essentially conical except very close to the orifice. Figure 1 represents a differential volume in a conical field. The equations are radial, and angular derivatives are zero. In the analytical development, solid sublimation and particle density variations are considered negligible compared with the liquid evaporation and particle size attenuation.

The continuity equation is written at a point (r,θ) in terms of the total mass flux, the local gas, and second-phase volume fractions,

$$\rho_s(1 - \alpha)v_s + \rho_g \alpha v_g = \dot{m}(r,\theta) \quad (2)$$

The equation of motion for each phase is expressed in terms of forces per unit of total system volume. Since there is no explicit time dependence, the time derivative reduces to a spatial derivative for the gas phase,

$$\rho_g \alpha v_g(dv_g/dr) = -g_c(dP/dr) - D/V \quad (3)$$

For the second phase,

$$\rho_s(1 - \alpha)v_s(dv_s/dr) = D/V \quad (4)$$

The drag force per volume is expressed by

$$D/V = (1 - \alpha)D/V_p = (1 - \alpha)C_D\rho(v_g - v_s)^2/2d$$

where $C_D \equiv$ ratio of drag force to the relative fluid inertia, $d_s \equiv V_p/A_p$, the mean cross-sectional diameter of the particle, and C_D is commonly tabulated as a function of Reynolds number. For isentropic gas expansion

$$v_g = v_{g*}\left[\frac{M^2(\gamma + 1)/2}{1 + M^2(\gamma - 1)/2}\right]^{1/2}$$

for $M \gg 1$,

$$v_g = v_{g*}\zeta \quad (5)$$

where $\zeta \equiv [(\gamma + 1)/(\gamma - 1)]^{1/2}$. The pressure decreases approximately as

$$P/P_0 = M^{-2\gamma/(\gamma-1)} \to 0 \text{ for } M \gg 1$$

Method of characteristics solutions for free-gas expansion into a vacuum show that these terminal values are attained within approximately one orifice radius. Therefore, the pressure acceleration, dP/dr, is of short duration; the terminal velocity ζv_{g*} is used as the initial velocity v_{g0} in the equations of motion.

The prominent change associated with the initial expansion of the gas phase is the density attenuation, which is reflected in an initial reduction in the gas phase mass flux,

$$\rho_{g0}v_{g0}/\rho_{g*}v_{g*} = \dot{m}_{g0}/\dot{m}_{g*} \equiv 1/\beta \quad (6a)$$

Using Eq. (6a) in the continuity equation, an initial value for the quality is obtained to be used in the equations of motion,

$$x_0 = x_*/[(1 - x_*)\beta + x_*] \quad (6b)$$

Equations (5) and (6b), used as initial conditions for the problem, absorb the effect of the initial pressure acceleration. Using the continuity equation to eliminate the spatially dependent gas density, Eqs. (3) and (4) reduce to Eqs. (7) and (8),

$$dv_g/dr = -[\Phi(1 - x)/x]dv_s/dr \quad (7)$$

$$dv_s/dr = C_D\dot{m}(r,\theta)x(v_g - v_s)^2/\Phi 2d_s v_g \quad (8)$$

where $\Phi \equiv 1 - \dot{m}(r,\theta)(1 - x)/\rho_s v_s$. The radial field of the mass flux is obtained from mass conservation,

$$\dot{m}(r,\theta) = \dot{m}_0(\theta)/y^2 \quad (9)$$

where $y \equiv r/r_0$, dimensionless radius. The mass conservation equation for evaporation of a single spherical particle is

$$\rho_s(dV_s/dt) = \rho_s v_s(dV_s/dr) = j_m \pi d_s^2 \quad (10)$$

The mass flux at the surface is related to the heat flux $\dot{q}$ by

$$j_m = \dot{q}/h_{fg} \quad (11)$$

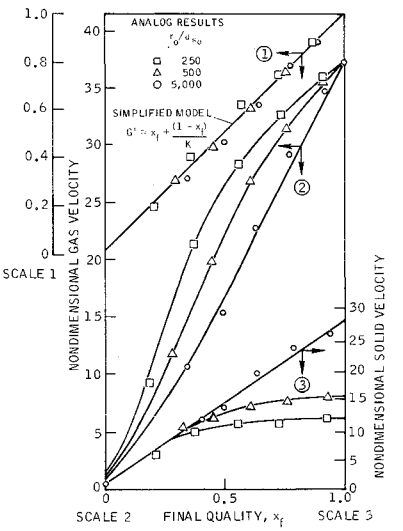

Fig. 2 Nondimensional velocities.

where $\dot{q}$ is a linear function of the particle surface temperature.[2] Solution of the diffusion equation for spherical particles yields eigenfunctions that decay exponentially in time. For steady flow, the time dependence appears as spatial variation; assuming a small velocity change with respect to a major surface temperature reduction, the surface temperature decays exponentially with distance. An approximate form for the heat flux is given by

$$\dot{q} \cong \dot{q}_0 e^{-\tilde{\lambda}(r - r_0)} \tag{12}$$

The spatial derivative of the particle volume V_s is expressed in terms of the quality and is substituted into Eq. (10). For large $\tilde{\lambda}$ there is a small change in v_s over one relaxation period; therefore, we obtain

$$(1 - x)^{-2/3}\, dx/dr \cong 3\tilde{\lambda}\Delta f(1 - x_0)^{1/3} e^{-\tilde{\lambda}(r - r_0)} \tag{13}$$

The relaxation constant $\tilde{\lambda}$ is obtained by using the total percentage mass attenuation that has occurred when evaporation ceases;

$$\lambda = 2\dot{j}_{m_0}/3\rho_s v_{s_0} d_{s_0} \Delta f \tag{14}$$

$$\Delta f = 1 - \delta_m{}^{1/3}, \quad x_f = 1 - \delta_m(1 - x_0) \tag{15}$$

The interphase mass transport is implicit in the spatial dependence of the quality;

$$x = 1 - (1 - x_0)\{1 - \Delta_f[1 - e^{-\lambda(r - r_0)}]\}^3 \tag{16}$$

Equations (7–9 and 16) completely define the radial flowfield.

The impingement force is evaluated using Newtonian impact theory, modified by an experimentally determined coefficient, C; $P_A = CP_N$. This coefficient, related to an accommodation coefficient for gas impingement, absorbs the deviations from Newtonian theory due to elastic collisions, surface irregularities, and surface evaporation. The Newtonian force is the sum of the momentum components of the flowfield normal to the surface; tangential components are unchanged. The multiphase momentum flux and local static pressure define the force on a surface element ΔA;

$$\Delta F_N = [(\cos^2\phi/g_c) \sum_{\text{phases}} m_i v_i + P_0]\Delta A \tag{17}$$

The static pressure P_0 is negligible;

$$P_N = \cos^2\phi \dot{m}_0(\theta) G/y^2 g_c \tag{18}$$

where $G \equiv xv_g + (1 - x)v_s$.

Analog Simulation and Solution

A complete radial field description for P_N requires the simultaneous solution to Eqs. (7, 8, and 16); this solution is used in the equation for G. Simulation of these equations on an analog computer provides exact solution. The following nondimensional variables are introduced into Eqs. (7) and (8), using Eq. (16) for the quality,

$$X = v_g/v_{g_0}, \quad Y = v_s/v_{s_0}, \quad Z_0 = x_0, \quad F = \xi + (1 - \xi)e^{-\theta' t}$$

$$\xi = 1 - \Delta_f, \quad \theta' = \lambda r_0 \quad k = v_{g_0}/v_{s_0}, \quad \lambda = \dot{m}_0(\theta)/\rho_s v_{s_0}$$

$$R_0 = r_0 C_D \lambda/2d_{s_0}k, \quad t = y - 1$$

Using Eq. (8) in Eq. (7), nondimensional Eqs. (19) and (20) result;

$$\dot{X} = R_0(1 - Z_0)F^2(kX - Y)^2/kXY(t + 1)^2 \tag{19}$$

$$\dot{Y} = R_0[1 - (1 - Z_0)F^3](kX - Y)^2/FX[Y(t + 1)^2 - \lambda(1 - Z_0)F^3] \tag{20}$$

where $(\dot{}) \equiv d(\ )/dt$. Let $G' \equiv G/v_{g_0}$. The nondimensional velocities X, Y, and G' are the necessary outputs from the analog.

Large values of the relaxation parameter θ' generate a need for two analog circuits: one for the initial solution, the near zone; and another for the steady-state or far zone. The near zone corresponds to the region where evaporation is in process; in the far zone, there is no interphase mass transport.

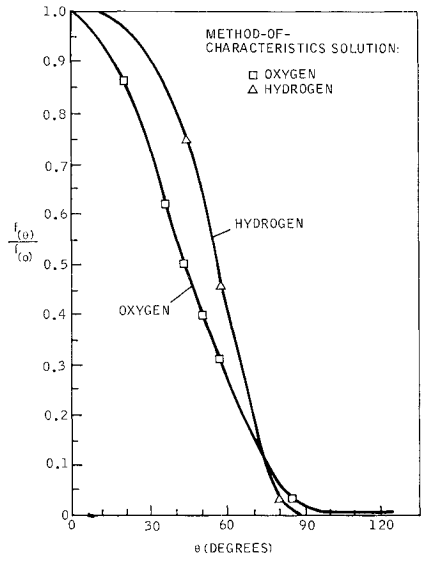

Fig. 3 Mass flux angular profile.

The parametric affects of R_0, Z_0, Δ_f, θ', and λ on the nondimensional velocity G' were studied for venting saturated liquid oxygen at 162.5°R. Liquid hydrogen parameter ranges are not as significant. Figure 2 shows the variations of G', X, and Y with final quality for different r_0/d_{s_0} ratios; G' reaches a terminal value within one radius.

The analog results for G' indicate that it has a linear form. Investigation of Eq. (7) establishes the functional dependence. Equation (7) is approximately given by

$$dv_g/dr = -[(1 - x)/x]\,[1 - \lambda(-x)v_{s_0}/v_s y^2]\, dv_s/dr$$

where

$$\lambda(-x)v_{s_0}/v_s y^2 < (1 - \alpha_0) \tag{21}$$

The inequality (21) becomes much stronger with increasing radius; the initial values are small: less than 0.5 for initial qualities greater than 5%. The differential equation rapidly approaches a limiting form. Integration for a constant quality yields

$$G' = x + (1 - x)/\zeta k_* \tag{22}$$

By using the final quality x_f, in Eq. (22), excellent agreement with the analog results is obtained; see Fig. 2. The Newtonian pressure is reduced to

$$P_N = \frac{\cos^2\phi \dot{m}_0(\theta) v_{g_*}}{g_c y^2}\left(\zeta x_f + \frac{(1 - x_f)}{k_*}\right) \tag{23}$$

The angular mass flux profile is represented by the ratio of the angular mass flux to the initial value of the total mass flow rate, $f(\theta) = \dot{m}_0(\theta)/\dot{m}_0$.

This equation is normalized by the mass conservation equation

$$1 = \int_0^{\theta_{\max}} f(\theta)\, \sin\theta d\theta \tag{24}$$

An approach to obtaining the functional dependence of $f(\theta)$ is to use the distribution associated with the isentropic gas expansion. Investigation of method-of-characteristics solutions to gas expansion for hydrogen and oxygen from converging nozzles resulted in an empirical relationship for the angular mass flux profile.

$$f(\theta)/f(0) = [1 - (\theta/\theta_{\max})^{5(\gamma - 1)}]^{2/(\gamma - 1)} \tag{25}$$

wherein $\theta_{\max} = (\zeta - 1)\pi/2$ is the maximum Prandtl-Meyer

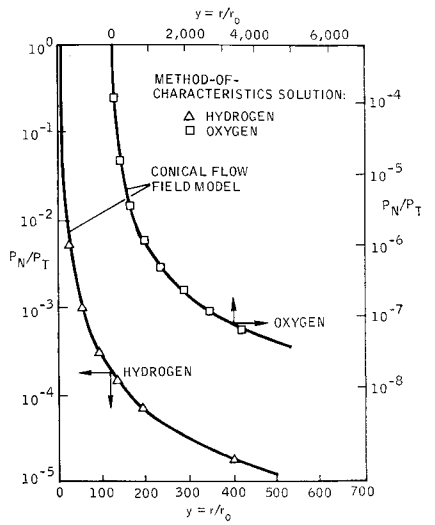

Fig. 4 Newtonian impingement pressure for 100% quality.

flow angle.[3] The curves in Fig. 3 are the angular dependences given by Eq. (25) for hydrogen and oxygen, and the symbols represent values from the method of characteristics solutions. The value of $f(0)$ is obtained from the normalization condition, Eq. (24). Values for $f(0)$ obtained by numerically integrating Eq. (24) were correlated using the relation: $f(0) = \zeta$. The angular profile of the mass flux for gas-dominated flow is

$$f(\theta) = \zeta\{1 - [2\theta/\gamma(\zeta - 1)]^{5(\gamma - 1)}\}^{2/(\gamma - 1)} \quad (26)$$

The attenuation coefficient β^{-1} is evaluated by comparing the two-phase model, for $x_f = 1.0$, with the all-gas Newtonian pressure, Eq. (1);

$$P_N/P_t = \beta^{-1}\gamma(\zeta/y)^2[(\gamma + 1)/2]^{\gamma/(1 - \gamma)} \quad (27)$$

$$\beta^{-1} = (0.75)^{2/(\gamma - 1)}\,(\gamma^2 - 1)^{1/(\gamma - 1)} \quad (28)$$

Using Eq. (28), a plot of P_N/P_t, for both Eq. (27) and Eq. (1), is shown in Fig. 4. For $y > 10$, the two expressions are in good agreement.

The final momentum flux is obtained using Eqs. (23) and (26),

$$P_N = \frac{\dot{M}_0 v_{g*}\zeta}{\pi r_0^2 g_c}\left[\zeta x_f + \frac{(1 - x_f)}{k_*}\right] S(y,\theta,\phi) \quad (29)$$

where $\dot{M}_0 = \dot{M}_{s*} + \dot{M}_{g*}/\beta$, and the function

$$S(y,\theta,\phi) = \left(\frac{\cos\phi}{y}\right)^2\left\{1 - \left[\frac{\theta}{(\pi/2)(\zeta - 1)}\right]^{5(\gamma - 1)}\right\}^{2/(\gamma - 1)} \quad (30)$$

contains all momentum flux field spatial dependence and impingement surface orientation. Separation of time and spatial dependence facilitates calculation of time-dependent forces and moments associated with the impingement surface kinematics. A digital computer program that couples the orifice thermodynamics with the vehicle kinematics implements this calculation.

Two-Phase Impingement Surface Coefficients

Effects of impingement surface conditions on the surface forces are evaluated by investigating each phase separately. Each phase is treated as a rarefied gas; this implies that the probability of reimpingement of previously scattered particles is small. The gas phase is developed using a one-particle distribution function with a Maxwellian velocity dependence translated by the macroscopic mean gas velocity in velocity space. The normal and tangential surface tractions[4] are expressed

$$P_{ng} = \alpha\rho_g v_g^2[\cos^2\phi(2 - f_n) + f_n\zeta(\pi/2\gamma)^{1/2}(T_{IS}/T_*)^{1/2} \times \cos\phi] \quad (31)$$

$$\tau_g = f_t\alpha\rho_g v_g^2 \sin\phi\cos\phi \quad (32)$$

where T_{IS} is the impingement surface temperature, and coefficients f_n and f_t represent the normal and tangential inelastic absorption of momentum by the impingement surface, respectively. For completely elastic scattering, $f_n = f_t = 0$; for complete absorption and re-emission by the surface, $f_n = f_t = 1$. The second term in Eq. (31) represents emission of the absorbed gas at a kinetic temperature equal to T_{IS}.

The solid phase is considered as a gas with zero-kinetic velocity (zero temperature). It is assumed that a particle either adheres to the surface on impact or its elastically scattered; the percentage that adheres [$100\,\mu(\phi)$] is a function of the flow properties, surface thermal and structural conditions, and the angle of incidence.

An induced momentum exchange results from the sublimation of solid that has deposited on the surface. The generated gas is assumed to have a Maxwellian velocity distribution and a kinetic temperature T_{RE}. Assuming instantaneous sublimation and no solid buildup on the surface, an approximate form for the total normal pressure is obtained,

$$P_{ns} = \rho_s v_s^2(1 - \alpha)[(2 - \mu)\cos^2\phi + \mu(\cos\phi)\xi] \quad (33)$$

where $\xi \equiv$ solid-phase momentum exchange coefficient $= (\pi RT_{RE}/2)^{1/2}/v_s \simeq$ (kinetic velocity of re-emitted gas)/(impingement velocity).

The tangential stress is given by

$$\tau_s = \rho_s v_s^2(1 - \alpha)\sin\phi\cos\phi[\mu]$$

Correction coefficients are defined for each phase,

$$C_{ng} \equiv 2 + f_n[(\pi T_{IS}/2\gamma\zeta^2 T_*)^{1/2}/\cos\phi - 1] \quad (34)$$

$$C_{ns} \equiv 2 + \mu[(\xi/\cos\phi) - 1] \quad (35)$$

$$C_{\tau g} \equiv f_t \cong f_n \qquad C_{\tau s} \equiv \mu \quad (36)$$

In the free molecular flow regime, $f_n \simeq f_t$.

Equations (29) and (30), coupled with Eqs. (34–36), yield the actual impingement tractions,

$$P_{nj} = C_j P_N \qquad \tau_j = C_{\tau j}\tan\phi P_N \quad (37)$$

where j = phase index.

The possible effect of the induced pressure, resulting from sublimation for the solid phase and re-emission for the gas phase, is illustrated by the following example: $\mu = f_n = 1$ (total adherence and absorption); $T_{RE} = 97°\text{R}$ (~triple point for oxygen); and $v_s = 250$ fps (possible velocity obtained from analog solution, $x_f = 20\%$). Assume a surface temperature of 200°R; then $T_{IS}/T_* = 200°/162.5° = 1.23$. With $\cos\phi = 1$, we obtain $C_{ng} = 1.48$, and $C_{ns} = 3.00$.

Thus, the induced momentum exchange from re-emission ($C_n - 1$) is 2.0 and 0.48 times the inelastic impact exchange for the solid and gas phases, respectively. This effect is enhanced by additional gas heating after sublimation. The conversion of impingement surface thermal energy to momentum transport is also an important consideration in the local heat-transfer effects. The gas-phase continuum effects, due to close proximity of the nozzle or for very large impingement surfaces at moderate distances, are approximately considered by neglecting reemission of gas particles: $T_{IS} \equiv 0$.

The parameter μ is greatly affected by T_{IS}. This dependence, along with the more subtle function of flowfield parameters, must be determined by an effective experimental program.

Conclusions

From this study of two-phase impingement effects of cryogenic propellant venting upon orbital vehicle dynamics, we

conclude that 1) time and spatial dependent variables in the two-phase impingement equation are separable; 2) our results agree well with method of characteristics solutions for gas expansion in a vacuum when the analytical model for 100% quality is used; and 3) it is important to consider the re-emission momentum exchange at the impingement surface for both the gas and solid phases; it is the same order of magnitude as the impact momentum.

References

[1] Walburn, A. B., "An Analytical and Experimental Examination of the Effect of Cryogenic Propellant Venting on Orbital Vehicle Dynamic Behavior," American Astronautical Society Southeastern Symposium in Missiles and Aerospace Vehicles Sciences, Dec. 1966.

[2] Schlichting, H., *Boundary Layer Theory*, McGraw-Hill, New York, 1960.

[3] Lipemann, H. W. and Roshko, A., *Elements of Gas Dynamics*, Wiley, New York, 1957.

[4] Hayes, W. D. and Probstein, R. F., *Hypersonic Flow Theory*, Academic Press, New York, 1959.

Re-Entry Dispersions Due to Atmospheric Uncertainties

GERALD R. WEISS*
IBM Federal Systems Division West, Westlake Village, Calif.

Nomenclature

A	=	reference area
c	=	sensitivity coefficient
C_D	=	drag coefficient
d	=	correlation distance
$E\{\ \}$	=	expected value operator
g	=	gravitational acceleration
g_c	=	mass-weight conversion factor
h	=	altitude
$\mathbf{P}$	=	covariance matrix
r	=	correlation coefficient
R	=	autocorrelation function
S	=	trajectory arc length
ΔS	=	arc length error
t	=	time
V	=	velocity
ΔV	=	velocity error
ω	=	white noise random variable
W	=	weight
ρ	=	density
$\Delta\rho$	=	density error
β	=	ballistic coefficient $- W/C_DA$
γ	=	flight-path angle referenced to local horizontal
σ^2	=	variance

Subscripts

i	=	ith atmosphere layer
0	=	initial conditions
s	=	arc length
x	=	downrange coordinate
y	=	vertical coordinate

Introduction

AN important factor in the evaluation of re-entry vehicle performance is the determination of trajectory dispersions due to geophysical environmental errors. For re-entry trajectories, a principal environmental error source is local variations in the atmospheric density. Present analytical techniques for determining atmospheric induced trajectory dispersions include the Sissenwine[1] density covariance method and the Purcell-Barbery[2] temperature covariance method. The fundamental equation used in both methods is

$$\sigma_s^2 = \sum_i \sum_j c_i c_j r_{ij} \sigma_i \sigma_j \tag{1}$$

where r_{ij} are the density correlation coefficients between ith and jth atmosphere layers in the density covariance method, and the temperature correlation coefficients between atmosphere layers in the temperature covariance method. Both methods require perturbation of the model atmosphere's discrete parameters to determine the influence coefficients c_i. The correlation coefficients are obtained by statistical reduction of meteorological data. The technique produces the covariance in the trajectory state at the specific altitude at which the influence coefficients are evaluated.

The purpose of this Note is to present an alternate technique for determining trajectory dispersions due to atmospheric uncertainties. The technique is termed the atmospheric random process method (ARP) because it assumes that the trajectory error state equations are forced by an atmosphere whose parameters are described by an exponentially correlated random process. The ARP technique results in a set of continuous differential equations for the variances of the trajectory state, the solution of which yields a continuous altitude history of the dispersion growth. The method is illustrated for the scalar trajectory variable, arc length, and the scalar atmospheric error source, density.

Atmospheric Density Model

The true density of the atmosphere at any altitude above the earth's surface is modelled as a mean value plus an additive noise term,

$$\rho_{\text{true}} = \rho_{\text{mean}} + \Delta\rho_{\text{noise}} \tag{2}$$

The autocorrelation function for the noise density is assumed to be

$$R(h,h + \Delta h) = E\{\Delta\rho(h)\Delta\rho(h + \Delta h)\} = \sigma^2(h)e^{-|\Delta h|/d} \tag{3}$$

where $\sigma(h)$ = standard deviation of the noise density, d = correlation distance of the noise density, and Δh = difference between any two altitudes.

Examination of statistically reduced meteorological data[1] for St. Paul Island, Alaska and Omaha, Nebraska for various seasons of the year reveals that, typically, the noise density standard deviation is not stationary with respect to altitude. Its value is, however, nearly proportional to the local mean density. The simulation results presented in this Note, thus, are based on a standard deviation given by

$$\sigma(h) = K\rho(h) \tag{4}$$

where K is varied between 1% and 5%. If the standard deviation of a specific local density profile is known, Eq. (4) may be replaced by a tabular value set during simulation.

Analysis

The perturbation equations for re-entry arc length are given by

$$d(\Delta S)/dt = \Delta V \tag{5}$$

$$d(\Delta V)/dt = (g_cV^2/2\beta)\Delta\rho \tag{6}$$

Changing the independent variable from time to altitude, the perturbation equations become

$$d(\Delta S)/dy = \Delta V/V \sin\gamma \tag{7}$$

$$d(\Delta V)/dy = (g_cV/2\beta \sin\gamma)\Delta\rho \tag{8}$$

$$d(\Delta\rho)/dy = -\Delta\rho/d + \omega(y) \tag{9}$$

Received May 19, 1969; revision received July 11, 1969.

* Staff Engineer, Guidance Software Department. Associate Member AIAA.